Influence of the electrode-electrolyte interface on electrochemical CO2 reduction reaction and hydrogen evolution reaction

Ye, C.

Citation

Ye, C. (2024, December 5). *Influence of the electrode-electrolyte interface on electrochemical CO2 reduction reaction and hydrogen evolution reaction*. Retrieved from https://hdl.handle.net/1887/4170871

Chapter 3

Influence of Cations on HCOOH and CO Formation during CO_2 Reduction on a $Pd_{ML}Pt(111)$ Electrode

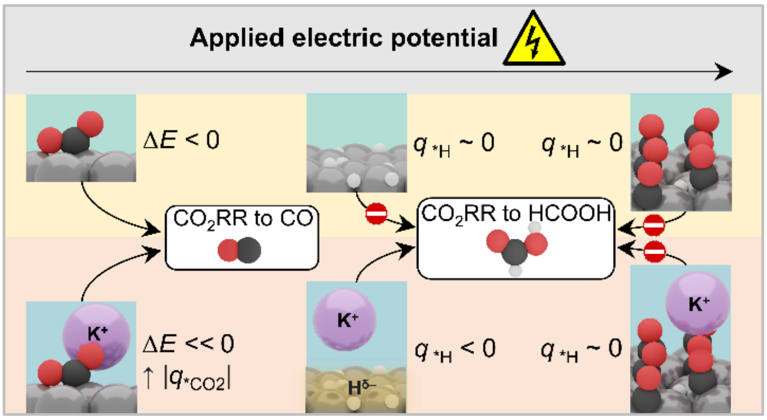

This chapter is based on:

Ye, C.; Dattila, F.; Chen, X.; Lopez, N.; Koper, M. T. M. *J. Am. Chem. Soc.* **2023**, 145 (36), 19601-19610.

Abstract: Understanding the role of cations on the electrochemical CO_2 reduction (CO_2RR) process is of fundamental importance for practical application. In this work, we investigate how cations influence HCOOH and CO formation on $Pd_{ML}Pt(111)$ in pH 3 electrolytes. While only (a small amount of adsorbed) CO forms on $Pd_{ML}Pt(111)$ in the absence of metal cations, the onset potential of HCOOH and CO decreases with increasing cation concentrations. The cation effect is stronger on HCOOH formation compared to CO formation on $Pd_{ML}Pt(111)$. Density functional theory simulations indicate that cations facilitate both hydride formation and CO_2 activation by polarizing the electronic density at the surface and stabilizing $*CO_2^{-}$. Although the upshift of the metal work function caused by high coverage of adsorbates limits hydride formation, the cation-induced electric field counterbalances this effect in case of *H species, sustaining HCOOH production at mild negative potentials. Instead, at the high *CO coverages observed at very negative potentials, surface hydrides do not form, preventing the HCOOH route both in absence and presence of cations. Our results open the way for a consistent evaluation of cationic electrolyte effects on both activity and selectivity in CO_2RR on Pd-Pt catalysts.

3.1 Introduction

The electrochemical carbon dioxide reduction reaction (CO_2RR) into fuels and chemicals has recently gained substantial attention as a promising method to utilize this abundant carbon feedstock and to store excess renewable electric energy. In aqueous media, the CO_2RR can generate various products, including formic acid (HCOOH), carbon monoxide (CO), hydrocarbons, and alcohols, depending on the catalyst and the microenvironment.[1-4] Therefore, understanding the factors determining selectivity at the molecular level is crucial to ensure the future application of CO_2RR.

The nature of the metal catalyst has an important effect on the activity and selectivity in CO_2RR. Of the monometallic catalysts, Cu exhibits a unique selectivity to methane and various multi-carbon products such as ethylene, ethanol, and propanol.[5-8] Precious metal catalysts such as Au and Ag show high selectivity towards CO in CO_2RR.[4, 9] Platinum-group metals, are also selective for CO formation but are affected by CO surface poisoning.[3, 10-12] Pd-based catalysts can reach a Faradaic efficiency of 95% for CO generation at negative potentials (-0.8 V_{RHE}).[10-11] However, this selectivity is potential dependent and Pd can also deliver a high Faradaic efficiency towards HCOOH (close to 99%) with a small overpotential of 0.1 V.[3] Although Pd deactivates over a few hours because of the simultaneous formation of (adsorbed) CO,[3] Pd is an excellent candidate to study the electrochemical CO_2RR because of this selectivity switch between HCOOH and CO formation in different potential windows.

To better understand the special reactivity of Pd for CO_2RR, detailed investigations on atomically well-defined Pd surfaces are highly desirable. Pt single crystals modified with a Pd monolayer are good candidates as their electrochemical and electrocatalytic properties have been shown to be similar to bulk Pd single crystals, but they do not exhibit the bulk-like hydrogen absorption of Pd crystals (a process which will mask the CO_2RR current).[13-15] Recent work has shown that a $Pd_{ML}Pt(111)$ single-crystal electrode has a high, almost reversible catalytic activity for the reduction of CO_2 to HCOOH and the oxidation of HCOOH to CO_2, very similar to bulk Pd crystals.[16] The high activity for the reduction of CO_2 to HCOOH at low overpotential was ascribed to the hydridic (negatively-charged) character of the surface adsorbed hydrogen $^*H^{\delta-}$ on $Pd_{ML}Pt(111)$, which reacts with CO_2 in the solution close to the metal to form HCOOH.[3, 16] This hydridic character was reported to depend on the metal work function.[3, 16] At more negative potentials, $^*CO_2$ binding through the carbon becomes more favorable, eventually leading to the formation of surface adsorbed *CO, which poisons the electrode.[16] Recently, surface polarization has been proposed as a crucial trigger for hydride transfer on transition metals.[17] Specifically, it was observed that more negative applied potentials increase the electrostatic potential drop at the metal/electrolyte interface, boosting the hydride transfer to acceptor molecules in the electrolyte.

Other than the nature of the catalyst, the electrolyte composition, especially the cations, has been shown to have a strong impact on the CO_2RR activity and selectivity.[18-22] On copper, silver, and gold electrodes,[22] it was observed that the reduction of CO_2 to CO does not occur in the absence of (alkali) cations in the electrolyte. This was ascribed to the stabilizing interaction between the cation and the first CO_2 reduction intermediate (negatively charged surface-adsorbed CO_2, denoted as $^*CO_2^{\delta-}$), although other effects of alkali cations have also been suggested (regulation of local pH and/or the local double layer electric field).[22] A $HCOO^-$-mediated pathway to CO has been proposed to occur on Ag(111) *via* outer-sphere cation activation of CO_2.[23] These observations make it relevant to investigate the cation effect on HCOOH formation, for which the $Pd_{ML}Pt(111)$ electrode is an ideal model system.

In this work, we present CO_2RR performance on a $Pd_{ML}Pt(111)$ electrode in a pH 3 electrolyte with various cation concentrations, focusing on selectivity differences between HCOOH and CO formation as a function of potential. We show that the onset potential for both HCOOH and CO formation shifts to more positive potential with the increase of the cation concentration. Remarkably, there is a differential effect in the reaction paths, the cation effect being stronger on HCOOH formation than on CO formation. Based on complementary density functional theory simulations, we present a mechanism to explain why HCOOH generation is highly sensitive to the presence of cations in the electrolyte under realistic conditions, *i.e.* high *H and *CO coverages. Our work underscores the crucial importance of cations and the overall microenvironment design in catalytic CO_2RR.

3.2 Experimental Section

Chemicals and cell preparation. Ultrapure water (resistivity > 18.2 MΩ·cm, Millipore Milli-Q) was used for all experiments in this work. Prior to each experiment, all cell compartments were cleaned by storing them in a potassium permanganate solution (1 g·L^{-1} $KMnO_4$ (Fluka, ACS reagent) in 0.5 M H_2SO_4 (Fluka, ACS reagent)) overnight. The solution was subsequently drained and the cell compartments were rinsed with a dilute piranha solution (1:3 v/v of H_2O_2 (Merck, Emprove exp) / H_2SO_4) to remove residual $KMnO_4$ and MnOx. Afterwards, the cell compartments were cleaned by repetitively rinsing and boiling with Milli-Q water to remove all inorganic contaminants. Electrolytes were prepared from $LiClO_4$ (Sigma-Aldrich, ≥ 99.99% trace metal basis), $NaClO_4$ (Sigma-Aldrich, ≥ 99.99% trace metal basis), $KClO_4$ (Sigma-Aldrich, ≥ 99.99% trace metal basis), $NaClO_4$ (Sigma-Aldrich, ≥ 99.99% trace metal basis), H_2SO_4 (Merck, Suprapur, 96%), $PdSO_4$ (Sigma-Aldrich, 99.99% trace metal basis) and $HClO_4$ (Sigma-Aldrich, Ultrapure, 70%). In this work, a Pt wire (0.5 mm diameter, MaTecK, 99.9%) was used as the counter electrode, a reversible hydrogen electrode (RHE) was used as the reference electrode, and all the potentials were iR corrected and controlled with an Autolab PGSTAT302N potentiostat.

Preparation of Pd monolayers on Pt (111) single crystal. The characterization and preparation of the electrodes were carried out in the hanging meniscus configuration in standard three-electrode glass cells. Prior to each experiment, argon (Linde, 5.0) was purged through the electrolyte for 30 min to remove air from the solution. The Pt(111) single crystal (area = 0.08 cm^2) was prepared according to the Clavilier method[24] and characterized with cyclic voltammetry in 0.1 M $HClO_4$. Cyclic voltammogram of Pt(111) in 0.1M $HClO_4$ measured at 50 mV s^{-1} is shown in Figure B.1a. Afterwards, the Pd monolayer was deposited on the Pt(111) single crystal with the method previously reported by our group.[16, 25] Briefly, the prepared Pt(111) single crystal was transferred and immersed into a Pd^{2+} containing electrolyte at +0.85 V_{RHE}, and then cycled between +0.07 and +0.85 V_{RHE} until a full monolayer of Pd was formed on Pt(111). The corresponding Pd formation process on Pt(111) is shown in Figure B.1b, with the growth of a sharp peak at 0.23 V_{RHE} representing the accumulation of Pd on the Pt(111) surface and a decreasing peak at 0.5 V_{RHE} which is the characteristic spike of Pt(111) in 0.1M H_2SO_4.[25] With the accumulation of Pd on Pt(111), the peak at 0.5 V_{RHE} eventually disappears, which suggests a full monolayer on Pt(111) surface. After Pd monolayer deposition, the $Pd_{ML}Pt(111)$ electrode was taken from the cell and rinsed with Milli-Q water thoroughly. Finally, the freshly prepared $Pd_{ML}Pt(111)$ was characterized in 0.1M $HClO_4$ and used as working electrode in the subsequent experiments.

Electrochemical measurements. All electrochemical experiments were carried out in a standard three-electrode electrochemical cell. The CO_2RR experiment in the absence of metal cations was performed in 1 mM $HClO_4$ (pH 3). pH=3 was chosen as it is the highest pH where one still has reasonable electrolyte conductivity in the absence of (alkali) cations, while having low proton reduction current. In case of electrolytes with different cation concentrations, calculated amounts of salt were added to 1 mM $HClO_4$ solution. Prior to each experiment, CO_2 (Linde, 4.5) was purged through the electrolyte for at least 30 min to obtain a CO_2-saturated electrolyte. Cyclic voltammetry measurements at 10 or 50 mV s^{-1} were first taken in pH 3 working electrolytes. Afterwards, linear sweep voltammetry measurements were performed from 0.1 V_{RHE} to the required negative potentials at 1 mV s^{-1}, followed immediately by CO oxidation stripping experiments taken at 10 mV s^{-1}. The scan rate for CO oxidation stripping experiments was chosen to oxidize all CO adsorbed on Pd surface in one scan. Due to the strong CO adsorption on Pd surface,[25] CO generated during CO_2RR remains on Pd surface until it is oxidized to CO_2 during the CO oxidation stripping experiments. With a known surface area of the electrode (the same surface area as Pt(111) single crystal) , the CO surface coverage generated during CO_2RR was then estimated from the CO oxidation charge obtained from the stripping experiments.[16, 26] In case of linear sweep voltammetry recorded in argon-purged electrolyte, argon was first purged through the electrolyte for at least 30 min to obtain an air-free electrolyte and then linear sweep voltammetry experiments were performed from 0.1 V_{RHE} to negative potential at a scan rate of 10 mV s^{-1}.

Online high-performance liquid chromatography (HPLC). All the online HPLC experiments were carried out in a H-type electrochemical cell equipped with three electrodes.

The cell compartments were separated by a Nafion 117 membrane. Prior to the online HPLC experiments, CO_2 (Linde, 4.5) was purged through the cell for at least 30 min to saturate the electrolyte. While a linear sweep voltammetry was performed from +0.1 V_{RHE} to the required negative potentials at 1 mV s^{-1}, liquid samples were simultaneously collected with an open tip positioned close to our working electrode at a collection rate of 60 μL min^{-1}.[27] Therefore, each sample contains products averaged over a potential range of 60 mV. Or in other words, each sample takes a collection time of 60 s. Afterwards, the collected samples were analyzed by HPLC equipped with an Aminex HPX-87H column (BioRad) and a RID detector (Shimadzu). Notably, the obtained HCOOH concentration in this work is a measure of the $HCOO^-$ concentration near the working electrode (which will be higher than bulk $HCOO^-$ concentration) and therefore not suitable for a quantitative Faradaic efficiency determination. Chronoamperometry experiments at -1.2 V_{RHE} were performed to check HCOOH formation in a pH 3 electrolyte in the absence of metal cations. The online-HPLC tip was positioned close to the working electrode. After 10 min of chronoamperometry, a liquid sample was taken and further analyzed with HPLC. A higher local HCOOH concentration (if there is any formed during CO_2RR) with chronoamperometry at fixed potentials is expected and detected with HPLC.

Density functional theory details. We performed the density functional theory (DFT) simulations through the Vienna Ab initio Simulation Package (VASP).[28-29] We employed the PBE density functional[30] including dispersion through the DFT-D2 method,[31-32] with our reparametrized C_6 coefficients.[33] Inner electrons were reproduced by PAW pseudopotentials[34-35] and the monoelectronic states for the valence electrons were expanded as plane waves with a kinetic energy cutoff of 450 eV. We modeled the experimental system in agreement with our recent works.[22, 36] The surface model for the cation-free case consisted of a (3×3) $Pd_{ML}Pt(111)$ supercell, including 1 Pd monolayer on top of 4 Pt layers, where the two bottom layers were kept fixed to the bulk distance (see Figure 3.5a-b). To assess the role of alkali cations, we introduced in the simulation cell a solvated K^+ (with 5 H_2O in its coordination shell), fixing its z-coordinate to a distance of 4 Å (near-cation) and 9 Å (far-cation) from the surface layer. We considered two systems with different cation-surface distance to decouple short- and long-range cation interactions. Besides, to assess the case of charged simulations cells,[37] we considered for both the near- and far-cation cases a cell with 1 excess electron (K^+ without $OH^–$) and a neutral cell (K^+ with $OH^–$). For the second system, K^+ was neutralized *via* a $OH^–$ formed by removing a hydrogen from one of the H_2O molecules.[22] The vacuum extended for at least 10 Å beyond cation's solvation shell (or the Pd surface layer, for the cation-free case). Since the solvation layer with cations, water molecules, and adsorbates was placed only on one side of the slab, an additional dipole correction was applied to remove spurious contributions arising from the asymmetric slab model.[38]

Effect of applied electric potential on formation energies. The thermodynamics of CO_2 activation was assessed by computing the formation energy of this intermediate (Equations 3.1-2). A CO_2 (1/9 ML) was let to adsorb on the surface. For the system with 4 Å distance between K^+ and surface, the adsorbate was initially placed in proximity of the alkali cation ($d_{K+\text{-}O(CO2)}$ ~ 2.80 Å)[39] to enable short-range cation effects. Formation energies were calculated taking as energy references CO_2(g), H_2O(g), and surface+solvation layer, *i.e.* $Pd_{ML}Pt(111)$ 3×3 + $K^+(5H_2O)$. To account for variations in the metal work function and consequent changes of electric potential along the reaction path, we first estimated DFT formation energies at the electrostatic potential Φ corresponding to the work function W of the environment. The electrostatic potential Φ was calculated by normalizing the work function by the unit of elementary charge $e^–$ ($–1e^–$).[40] E and Φ indicate respectively DFT energies and electrostatic potential for surface + solvation + adsorbate (ads) and surface + solvation alone (surf), as reported in Table B.1, while q represents the surface charge density for initial state (surface + solvation) and final state (surface + solvation + adsorbate), see Table B.2. Next, we computed all energies at the work function corresponding to an applied electric potential of -0.40 V vs RHE (*i.e.* -0.58 V vs SHE at pH = 3) through Equation 3.2.[41] Given that the work function for the standard hydrogen electrode is 4.4 eV,[40] at an applied potential of -0.4 V vs RHE the expected metal work function is 3.82 eV. Δq represents the change in surface electronic charge along the reaction step and it is given in unit of elementary charge $e^–$ ($– 1\ e^–$).

$$E_{\mathrm{ads}}(\Phi_{\mathrm{surf}}) - E_{\mathrm{surf}}(\Phi_{\mathrm{surf}}) = E_{\mathrm{ads}}(\Phi_{\mathrm{ads}}) - E_{\mathrm{surf}}(\Phi_{\mathrm{surf}}) + \frac{(q_{\mathrm{ads}}-q_{\mathrm{surf}})(\Phi_{\mathrm{ads}}-\Phi_{\mathrm{surf}})}{2} \tag{3.1}$$

$$\Delta E(\Phi_{-0.4\ \mathrm{V\ vs\ RHE}}) = \Delta E(\Phi_{\mathrm{surf}}) + \Delta q(\Phi_{\mathrm{surf}} - \Phi_{-0.4\ \mathrm{V\ vs\ RHE}}) \tag{3.2}$$

3.3 Results and Discussion

3.3.1 Results

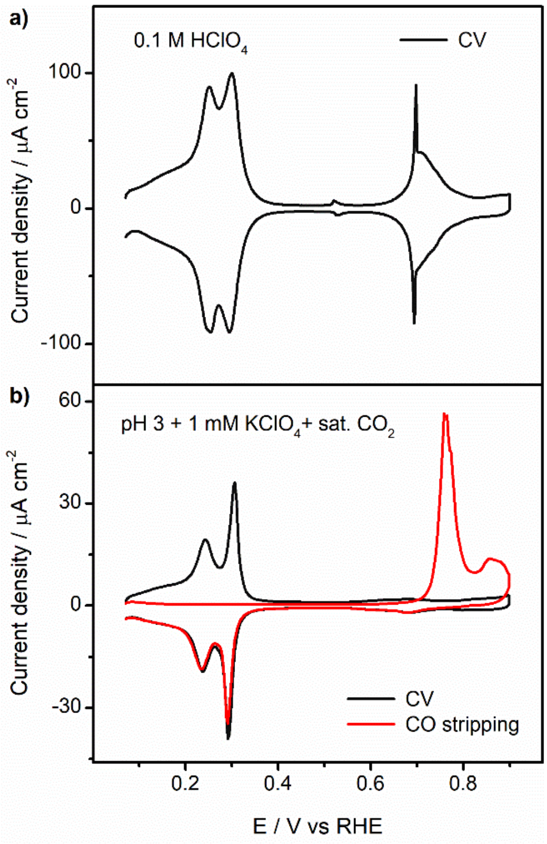

Figure 3.1 Cyclic Voltammetry of Pd$_{\mathrm{ML}}$Pt(111). a) Cyclic voltammogram of Pd$_{\mathrm{ML}}$Pt(111) electrode in 0.1M HClO$_4$. Scan rate: 50 mV s^{-1}. b) Blank cyclic voltammograms (black) and CO stripping voltammogram (red) of Pd$_{\mathrm{ML}}$Pt(111) in CO$_2$-saturated pH 3 electrolyte in the presence of 1 mM KClO$_4$. Scan rate: 10 mV s^{-1}.

Cyclic voltammetry of PdMLPt(111). Figure 3.1a shows the blank cyclic voltammogram of Pd$_{\mathrm{ML}}$Pt(111) in 0.1M HClO$_4$. The blank curve, measured at 50 mV s^{-1}, shows the characteristic regions of the Pd$_{\mathrm{ML}}$Pt(111) electrode: a region between +0.05 and +0.35 V$_{\mathrm{RHE}}$

with peaks at +0.21 and +0.31 V_{RHE}, corresponding to the replacement of adsorbed *H by adsorbed *OH and the replacement of adsorbed *OH by adsorbed $*ClO_4^-$, respectively; a low-current region between +0.35 and +0.65 V_{RHE} in which the surface is covered with adsorbed perchlorate anions (which appear to undergo a structural transition at ca. +0.52 V_{RHE}); and a region between +0.65 and +0.90 V_{RHE} with a sharp peak at +0.69 V_{RHE}, which is ascribed to the replacement of adsorbed $*ClO_4^-$ by a higher coverage of *OH adsorption or *O adsorption.[16, 25] The blank voltammetry in Figure 3.1a confirms the deposition of a single Pd monolayer on the Pt(111) single crystal as well as the cleanliness of the electrolyte, thereby ensuring the robustness and reproducibility of the experiments in this work.

There are small changes and shifts in these peaks for a pH 3 electrolyte in the absence and presence of cations, which have been described in detail in a previous work.[25] Figure 3.1b shows the blank cyclic voltammogram of $Pd_{ML}Pt(111)$ in a pH 3 electrolyte with 1 mM $KClO_4$ in the presence of CO_2. CO_2 leads to the presence and adsorption of bicarbonate (HCO_3^-) on $Pd_{ML}Pt(111)$. As shown in black curve in Figure 3.1b, the peak at +0.31 V_{RHE} increases in sharpness (compared with the peak at +0.21 V_{RHE}), while the stronger bicarbonate adsorption, compared to perchlorate adsorption, lowers the current density in the potential window from +0.35 to +0.9 V_{RHE}, *i.e.* it suppresses *OH and/or *O adsorption.[25] Importantly, below +0.1 V_{RHE}, the $Pd_{ML}Pt(111)$ electrode is fully covered with adsorbed hydrogen.

Voltammetry is also used to estimate the amount of adsorbed carbon monoxide (*CO) formed on the $Pd_{ML}Pt(111)$ electrode during CO_2RR experiments. To this end, we use CO stripping voltammetry. The red curve in Figure 3.1b shows the oxidative stripping voltammogram of a full saturation coverage of *CO obtained from CO_2RR on the $Pd_{ML}Pt(111)$ electrode, which corresponds to ca. 0.75 ML in terms of available Pd surface atoms. *CO remains on the surface of the $Pd_{ML}Pt(111)$ electrode after CO_2RR, which blocks the electrode surface and results in a low current observed in the region between +0.05 and +0.35 V_{RHE} at the beginning of oxidative stripping voltammogram. With more positive potential, CO oxidation peaks between 0.65 V_{RHE} and 0.90 V_{RHE} are observed. Upon oxidation of adsorbed *CO, the typical CV features in pH 3 electrolyte are again observed in the negative going scan. This means that the $Pd_{ML}Pt(111)$ electrode should still be intact and can be used again for a new experiment.

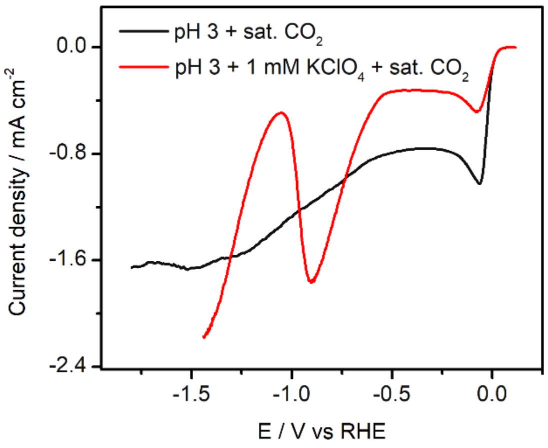

Figure 3.2 Linear Sweep Voltammetry of $Pd_{ML}Pt(111)$ in CO_2 saturated pH 3 electrolytes in the absence (black) and presence of 1mM $KClO_4$ (red). Scan rate: 10 mV/s.

Cation effect on HCOOH and CO formation during CO_2RR. After surface characterization, we studied the cation concentration effect on formic acid and CO formation during CO_2RR on $Pd_{ML}Pt(111)$ in pH 3 electrolytes. The CO_2RR experiments were carried out by linear sweep voltammetry, scanning from +0.07 V_{RHE} to different negative vertex potentials at 1 mV s^{-1}. HCOOH and CO production during CO_2RR was obtained from online HPLC and CO stripping voltammetry respectively, as introduced in the experimental section and the previous section. Figure 3.2 shows the corresponding linear sweep voltammograms, obtained at higher scan rate (10 mV/s). The meaning of the effect of 1 mM $KClO_4$ on the voltammetry is explained in the following sections. All CO stripping voltammograms obtained in this work are shown in Figures B.3 - B.7 in the Supporting Information.

Figure 3.3 shows the obtained CO coverage and HCOOH production during CO_2RR on $Pd_{ML}Pt(111)$ as a function of potential in a pH 3 electrolyte, in the presence of 0, 1 and 99 mM $KClO_4$ respectively (additional data for pH 3 with 5 and 10 mM $KClO_4$ are shown in Figures B.5 and B.6, a comparison is provided in Figure B.8). Figure 3.3a shows CO and HCOOH production in the absence of metal cations. CO is observed on $Pd_{ML}Pt(111)$ in the

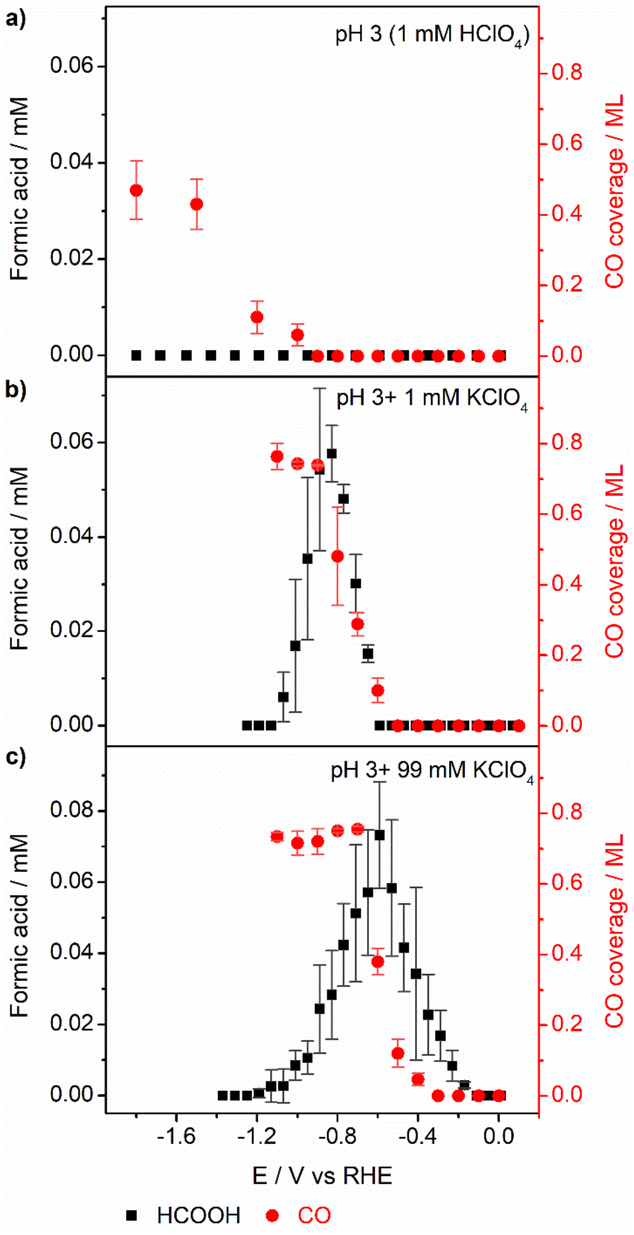

Figure 3.3 Cation concentration effect on CO_2RR on $Pd_{ML}Pt(111)$. CO coverage and HCOOH formation during CO_2RR obtained in CO_2 saturated pH 3 electrolytes a) in the absence of metal cations, in the presence of b) 1 mM $KClO_4$ and c) 99 mM $KClO_4$. Error bars are standard deviations based on three independent measurements.

absence of metal cations, albeit at a considerably negative onset potential of -1.0 V_{RHE}. The obtained maximum CO coverage under these conditions is ca. 0.4 ML at -1.8 V_{RHE}, which is much lower than the saturation CO coverage reported before.[16] Remarkably, no HCOOH production was observed in the absence of metal cations. To verify this result, 10 min of chronoamperometry was also carried out at -1.2 V_{RHE} with online HPLC, and indeed no HCOOH was detected (see Figure B.3b). Although reporting Faradaic Efficiencies (FE) is not the goal of this work, note that the amount of HCOOH formed is below the limit of detection for HPLC, whereas that of CO (determined by stripping voltammetry) is not, at the more negative potentials. However, the CO that we detect is adsorbed CO, not dissolved CO. We have no (voltammetric) evidence for the formation of dissolved CO under the conditions of our experiment.

Figures 3.3b, c show the same experiments with different concentrations of metal cations in the electrolyte. Figure 3.3b shows CO and HCOOH formation during CO_2RR in the electrolyte with the presence of 1 mM $KClO_4$. *CO is produced with an onset potential of -0.6 V_{RHE}, whereas the formation of HCOOH was observed with a slightly more negative onset potential of -0.65 V_{RHE}. With the increasingly negative-going potential, *CO coverage and HCOOH formation keep increasing until a high *CO coverage (ca. 0.74 ML) is reached at -0.9 V. From -0.9 V_{RHE} and more negative potentials, the *CO coverage remains constant while HCOOH formation drops due to the high coverage of *CO on the surface. Compared with CO_2RR in pure pH 3 electrolyte, it is clear that the onset potential of CO_2RR is less negative in the presence of 1mM $KClO_4$. With the increase of the cation concentration (99 mM $KClO_4$, Figure 3.3c), CO formation starts at -0.4 V_{RHE} whereas HCOOH is produced from -0.2 V_{RHE}. This result shows that cations have a stronger effect on HCOOH production compared to *CO formation, yielding a lower overpotential for HCOOH in the presence of a high cation concentration. This result is consistent with HCOOH as the major CO_2RR product (with minor CO poisoning) at low overpotentials, as shown in previous work on nanoparticulate Pd. Note that on nanoparticulate Pd, the current due to H intercalation should be minimal, at least during long-term electrolysis experiments.[3]

Knowing the effect of cations of CO_2RR on $Pd_{ML}Pt(111)$, we can now understand the voltammograms in Figure 3.2. The reduction wave between 0 and -0.5 V_{RHE} is due to the (diffusion-limited) reduction of protons (their concentration being ca. 1 mM at pH=3). The current density is higher in the absence of cations (black curve) as under these conditions, protons are also transported to the surface by migration, in addition to diffusion.[42-43] In the presence of cations (red curve), CO_2 reduction starts after -0.5 V_{RHE}. The corresponding peak is completely absent when cations are lacking. The peak shape is caused by the fact that at potentials more negative than -0.9 V_{RHE}, adsorbed CO is formed and the production of HCOOH is inhibited. To confirm the origin of the peak at -0.8 V_{RHE}, linear sweep voltammetry was carried out under the same experimental conditions in argon-purged pH 3 electrolyte. The corresponding linear sweep voltammogram is shown in Figure B.2. No peak was observed in pH 3 electrolyte with the presence of 1 mM $KClO_4$, confirming that the peak at -0.8 V_{RHE} is due to CO_2 reduction.

Interestingly, at potentials more negative than -1.1 V_{RHE}, the solution with cations clearly shows the reduction of water. There is no such clear water reduction current in the absence of cations. One could interpret this as an important promoting role of cations of water reduction (an effect which is known),[44] but one should also be aware that in the absence of supporting electrolyte, there are no ions available to carry such a reduction current. Therefore, we cannot claim that water reduction does not occur without cations, only that cations promote water reduction.

Furthermore, we also studied the effect of cation identity on CO and HCOOH formation during CO_2RR on $Pd_{ML}Pt(111)$. Figure 3.4 shows the obtained CO coverage and HCOOH production during CO_2RR as a function of potential in pH 3 electrolytes in the presence of 99mM $LiClO_4$ and $NaClO_4$, respectively. We observe that the CO coverage obtained from pH 3 electrolyte containing 99 mM $LiClO_4$ is ca. 0.5 ML, which is less than the coverage obtained in the pH 3 electrolyte containing 99 mM $NaClO_4$ or $KClO_4$. Moreover, we observe a correlation between CO_2RR activity and the cation identity. The activity for CO and HCOOH formation on $Pd_{ML}Pt(111)$ increases in the order $Li^+ < Na^+ < K^+$, following the ability of these species to accumulate near the surface.[22, 36] These results confirm the specific importance of the nature of the metal cations, and that in general, a strongly hydrated cation such as Li^+ has a lower promoting effect on CO_2 activation compared to more weakly hydrated cations.

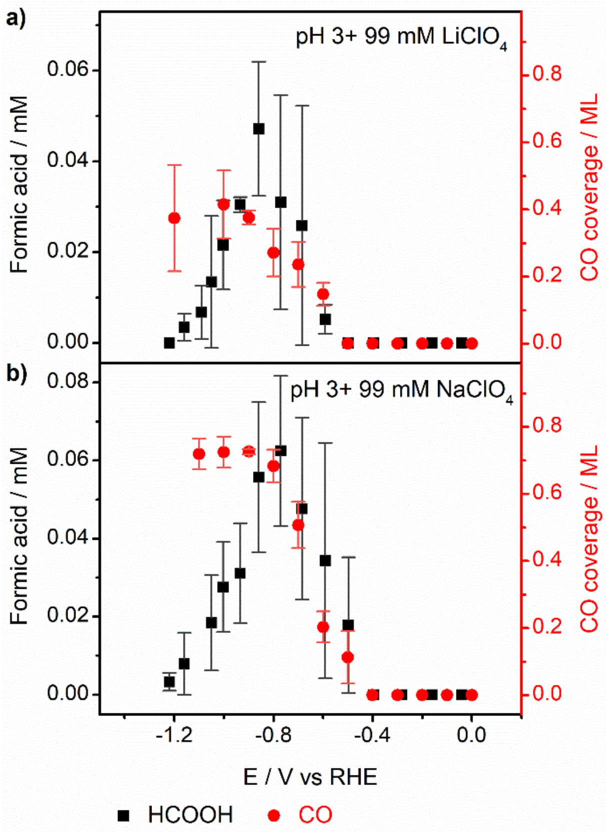

Figure 3.4 Cation identity effect on $Pd_{ML}Pt(111)$. CO coverage and HCOOH formation during CO_2RR obtained in CO_2 saturated pH 3 electrolytes containing 99 mM a) $LiClO_4$ and b) $NaClO_4$. Error bars are standard deviations based on three independent measurements.

Computational model. To gain additional insights into the mechanism underlying the observed cation effects on HCOOH and CO formation during CO_2RR, we carried out complementary density functional theory (DFT) simulations. According to the state-of-the-art, the mechanisms for the formation of formic acid and CO from CO_2RR encompass several elementary steps. For CO_2 reduction to formic acid on Pd, it is now agreed that the most relevant step is the adsorption of hydrogen as hydride ($*H^{\delta-}$),[3, 16] which performs a nucleophilic attack on the positively charged carbon of a nearby CO_2 in solution. Depending on the bulk solution pH, the generated formate becomes protonated to formic acid. Instead, the route towards CO requires the adsorption of CO_2 *via* the C atom, with subsequently one of the terminal O atoms becoming hydrogenated until water splits off, leaving adsorbed *CO on the catalyst surface.

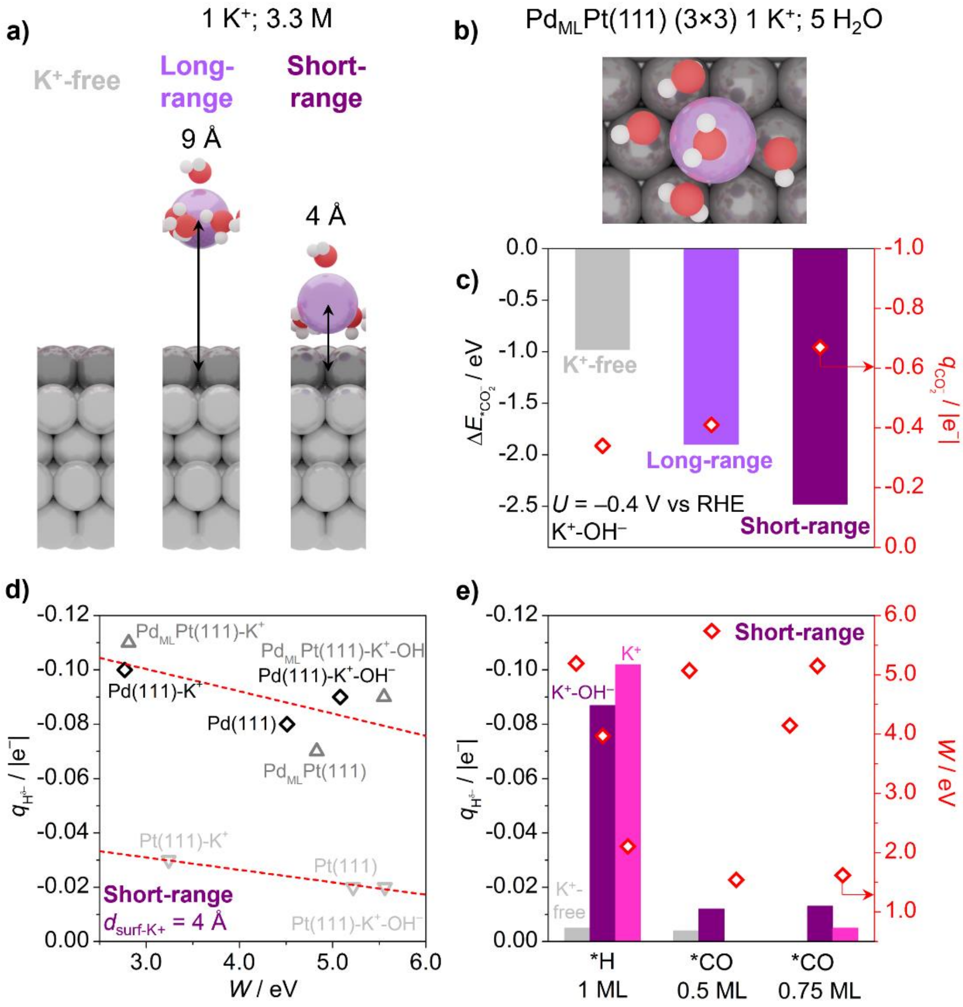

Figure 3.5 Cation promotional effect on CO_2 adsorption and formation of a surface hydride ($*H^{\delta-}$). a) Side and b) top views of the $Pd_{ML}Pt(111)$ (3×3)-1K^+(5 H_2O) models. c) CO_2^- formation energy at U = -0.4 V vs RHE (left y-axis) and excess charge on CO_2 unit (right *y*-axis) for a neutral $Pd_{ML}Pt(111)$ (3×3)-1K^+(5 H_2O) supercell (K^+-OH^- couple). d) Correlation between $H^{\delta-}$ Bader charges and work function (W) of Pd(111) (3×3), $Pd_{ML}Pt(111)$ (3×3), and Pt(111) (3×3), respectively black, dark and light gray data points. For both charged (K^+) and neutral supercells (K^+-OH^-), the cation-surface distance was 4 Å. e) $H^{\delta-}$ Bader charges (left *y*-axis) and metal work function (red data points, right *y*-axis) for $Pd_{ML}Pt(111)$ (3×3) at various *H and *CO coverages. Gray, purple, and magenta columns indicate respectively the K^+-free, neutral (K^+-OH^-), and charged (K^+) supercells. When present, the cation was placed 4 Å far away from the surface.

To model these key reaction steps, we carried out DFT simulations with the PBE-D2 functional.[30-33] To simulate the experimental surface without cation in the electrolyte, we chose a (3×3) $Pd_{ML}Pt(111)$ supercell, composed of 1 Pd monolayer on top of 4 Pt layers, of which the two lower layers were kept fixed to resemble the bulk. Further, to assess the role of metal cations, we included 1 K^+ with 5 coordinated H_2O molecules within its solvation shell in the simulation cell.[36] Since the volume of the solvation layer accounts for 0.50 nm^3 (7 Å thickness), the surface cation concentration was equivalent to 3.3 M. K^+ was inserted at two fixed distances either 4 Å or 9 Å from the $Pd_{ML}Pt(111)$ surface (Figure 3.5a-b) to decouple short- and long-range cation effects on reaction intermediates. To avoid artificial interactions between periodic images, the vacuum thickness extended for 10 Å beyond the $Pd_{ML}Pt(111)$ surface layer for the cation-free case, and beyond the outermost water molecule if the cation was present, respectively.[45] Since we recently highlighted the importance of charged simulation cells to model cation effects,[37] we considered here both a cell with 1 excess electron (K^+ without $OH^–$) and a neutral cell (K^+ with $OH^–$). In this second case, we neutralized K^+ *via* a $OH^–$ formed by removing a hydrogen from one of the H_2O molecules.[22] Since excess electrons in the simulation cell led to significant variations in the metal work function W and consequently in the electrostatic potential Φ along the simulation cell (Figures B.9 and B.10), when assessing the thermodynamics of CO_2 activation (Figure 3.5c), we opted for neutral supercells (K^+-$OH^–$ couple) to keep W constant (as shown in Table B.1).

Mechanism of cation effect on CO_2 activation. CO_2 activation is often assumed as the rate-determining step for CO_2RR on transition metals.[22] To assess the potential role of cations on CO_2 reduction to CO, we estimated the energy required for activating CO_2 on $Pd_{ML}Pt(111)$ (3×3) for the cation-free case (see Equation 3.3) and in presence of cations at 4 and 9 Å far away from the surface (Equation 3.4). We corrected the DFT energy for a potential-dependent term calculated at U = -0.4 V vs RHE (pH = 3), the observed onset potential for CO_2 reduction to CO (Figure 3.3c). Such potential-dependent term was obtained by tuning the metal work function in line with the approach suggested by Chan and Nørskov (Refs. [40-41], as shown in section: Effect of Applied Electric Potential on Formation Energies, Equations 3.1 and 3.2, Tables B.1 and B.2). In Equation 3.5, Δq represents the change in electronic surface charge for $Pd_{ML}Pt(111)$ (3×3) between the final (surface + $*CO_2^-$) and initial (surface + CO_2) state, thus it is equal to -1 e^-.

$$CO_2 + e^- \rightarrow * CO_2^- \qquad \text{Equation 3.3}$$

$$CO_2 + K^+(5H_2O) + e^- \rightarrow * CO_2^- + K^+(5H_2O) \qquad \text{Equation 3.4}$$

$$\Delta E_{*CO_2^-}(\Phi_{-0.4\,\mathrm{V\,vs\,RHE}}) = \Delta E_{*CO_2^-}(\Phi_{\mathrm{surf}}) + \Delta q(\Phi_{\mathrm{surf}} - \Phi_{-0.4\,\mathrm{V\,vs\,RHE}}) \qquad \text{Equation 3.5}$$

In the presence of proximal metal cation ($d_{K+\text{-surf}}$ = 4 Å), the K^+ coordinates to the free oxygen of the CO_2 molecule, leading to a strong CO_2 binding (ΔE = -2.5 eV, as reported in Figure 3.5c). Instead, for a cation-surface distance of 9 Å, we observe a weaker $*CO_2$ adsorption energy, around -1.9 eV. In agreement with experimental results (see Figure 3.3a), CO_2 activation occurs also for the cation-free case, being exothermic by around -1.0 eV at -0.4 V vs RHE. Additionally, our results show that metal cations enhance the electron transfer from $Pd_{ML}Pt(111)$ to adsorbed CO_2 (see right *y*-axis in Figure 3.5c). In fact, the CO_2 Bader charge (q_{CO2}) is -0.67 $|e^-|$ for $d_{K+\text{-surf}}$ = 4 Å, while decreases to -0.41 $|e^-|$ if the cation is far from the surface ($d_{K+\text{-surf}}$ = 9 Å). q_{CO2} further reduces to -0.34 $|e^-|$ in absence of metal cations in the simulation cell. Cation-promoted electron transfer to CO_2 was confirmed as well on Pd(111) (3×3) and Pt(111) (3×3), see Figure B.11.

Mechanism of cation effect on hydride formation. Moving on to HCOOH selectivity, we assess the effect of cations on the formation of adsorbed hydride ($*H^{\delta-}$). As shown in Figure 3.5d, the Bader charge of adsorbed hydride ($*H^{\delta-}$) correlates with the work function of Pd(111), $Pd_{ML}Pt(111)$, and Pt(111), in line with previous findings in Ref. [3, 16]. In turn, the metal work function decreases in presence of neighboring K^+ due to increased cation-induced polarization of the surface electronic density, favoring the formation of surface hydrides. Such phenomenon may be also expressed in terms of metal *d*-band center. For materials with low *d*-band center, such as Pt(111) (ε_d ~ -2.0 eV), the limited electronic density available at the surface prevents an effective formation of a hydride ($\delta-$ ~ -0.02 $|e^-|$). Instead, on metals characterized by higher values of *d*-band center (ε_d ~ -1.5 eV, or low work function), such as

Pd(111) and Pd$_{ML}$Pt(111), more electronic density is available at the surface, enabling the formation of surface hydrides ($\delta-$ ~ -0.10 $|e^-|$). A previous experimental study showed a strong correlation between Pd content and HCOOH/HCOO$^-$ selectivity on Pt-Pd nanoparticles and aerogels, while pure Pt was reported not able to reduce CO_2 to HCOOH/HCOO$^-$.[16, 27, 46] We here confirm that CO_2RR to HCOOH requires hydride species on PdPt catalysts, which occur only for suitable surface charging, *i.e.* appropriate filling of *d*-band states or induced by neighboring cation. In fact, we observe that $*H^{\delta-}$ Bader charges correlate with the K$^+$-induced electric field (proportional to $q^{K+}/r^2_{K+\text{-}H}$), as shown in Figure B.12 and Table B.3. Higher intensities of cation-induced electric field lead to increased polarization at the surface[17], which enhances the hydridic character of *H.

Figure 3.5d suggests that surface hydrides should also form in absence of cations, which is at odds with experimental results on HCOOH selectivity for Pd$_{ML}$Pt(111) (Figure 3.3a). Thus, we upgraded our model to more realistic conditions, *i.e.* high *H and *CO coverages, retrieving input geometries from a previous theoretical study.[47] Remarkably, hydrides are preserved at 1 ML *H coverage only in presence of neighboring cations, while $\delta- > -0.01\ |e^-|$ in the cation-free case (Figure 3.5e). High CO coverages (0.5 and 0.75 ML) hinder the formation of surface hydrides both in absence and presence of alkali cations. Both insights can be rationalized by the upshift of Pd$_{ML}$Pt(111) work function at high adsorbate coverages, partially balanced by the downshift in presence of neighboring cation at high *H coverage (Figure 3.5e). Other factors may also contribute to the selective reduction of CO_2 to HCOOH on Pd$_{ML}$Pt(111) at mild negative potentials. Considering the case of outer-sphere CO_2 activation to HCOO$^-$ by alkali cations, proposed by Pidko *et al.*[23] on Ag(111), such coupling is exothermic for both neutral (K$^+$–OH$^-$) and charged (K$^+$) cells (see Figure B.13) on Pd$_{ML}$Pt(111) (3×3). Instead, for the cation free case, such process is endothermic by 0.2 eV. Nevertheless, in the case of adsorbed hydride transfer to physisorbed CO_2 at -0.4 V vs RHE, the cation contribution appears less critical. In fact, such step is almost thermoneutral (~0.1 eV) both in presence and absence of neighboring cations (Figure B.13).

3.3.2 Discussion

Our results show the crucial role of metal cations on HCOOH and CO formation during CO_2RR on $Pd_{ML}Pt(111)$. Without metal cations, only limited CO_2 reduction to CO takes place.[22] This result is slightly different from the previous work reported by our group for CO_2 activation to CO on Ag, Au, and Cu electrodes, for which cations are a necessary reaction partner. This difference must due to the fact that palladium binds CO more strongly, and therefore, the activation barrier for CO formation is lower, such that even in the absence of cations, CO formation can take place. The activity towards HCOOH and CO improves with the increase of cation concentration, leading to the decreased onset potential of both products. Remarkably, $Pd_{ML}Pt(111)$ produces no HCOOH in the absence of cations while it is still somewhat active for *CO formation. In the presence of a high cation concentration, the selectivity pattern reverses and HCOOH formation happens at a lower overpotential, suggesting a stronger cation effect on HCOOH formation than CO formation on $Pd_{ML}Pt(111)$. In a previous work, we have rationalized the role of $*H^{\delta-}$ on $HCOO^-$/HCOOH formation on Pd surfaces and the dependence of hydridic character on the metal work function.[16] Hydrides are instrumental for reducing CO_2 to $HCOO^-$/HCOOH on Pt-Pd catalysts through a nucleophilic attack on a nearby CO_2.

The insights from our DFT simulations support the mechanism reported for CO vs $HCOO^-$/HCOOH competition on $Pd_{ML}Pt(111)$,[16] complementing our previous observations on other transition metals (Ag, Au, Cu).[22] Neighboring cations ($d_{K+\text{-surf}}$ = 4 Å) enhance CO_2 activation by more than 1 eV at U = -0.4 V_{RHE} vs the cation-free case, further facilitating the electron transfer to the CO_2 unit (CO_2 Bader charge of -0.67 $|e^-|$). Regarding formic acid/formate selectivity, hydrides are effectively formed on materials with a low work function, such as Pd(111) and $Pd_{ML}Pt(111)$. These catalysts enable the transfer of surface electronic density to the adsorbate, while hydrides are not formed on catalysts with deep electronic states, such as Pt(111), which prevent the formic acid pathway. In case of a high *H coverage, the cation-induced local electric field counterbalances the upshift of the metal work function due to the adsorbates, which instead hinder the formation of hydrides for the cation-free case. Such evidence rationalizes one of the most striking experimental observations in this work, *i.e.* the complete absence of HCOOH formation in the absence of cations.

In addition to *H coverage effect, cation-induced outer-shell CO_2 activation and short-range stabilization of $HCOO^-$ may also aid in favoring HCOOH formation.[23] However, given the general agreement that HCOOH selectivity crucially depends on hydrides, we highlight here the stabilization of the hydridic character as the critical contribution of cations. We note that cations enhance the formation of surface hydrides and the hydride transfer to CO_2 by inducing a further polarization of the Pd-H bond, in line with the conclusions of ref 17. Finally, during CO_2RR, the interfacial pH changes[20, 48], which may impact interfacial reactivity. Previous reported work suggests a pH swing close to an Au electrode from bulk pH conditions to an interfacial pH around 10-12 during CO_2RR under highly reactive conditions.[20, 48] Cations have a small buffering capacity[21], with an impact on the interfacial pH which can be measured.[48] This effect may be one of the factors contributing to our experimental results, however, it is hard to imagine that this relatively small effect would explain the observations shown in Figure 3.3.

3.4 Conclusions

We have studied the cation effect on HCOOH and CO formation during CO_2RR with a well-defined Pt(111) electrode with epitaxially grown Pd monolayer. The experiments show that cations have a stronger effect on HCOOH formation compared to *CO formation. There is no HCOOH formation in the absence of cations though there is *CO formation at high overpotentials. In the presence of a high cation concentration a lower overpotential for HCOOH formation is observed. Our DFT results help rationalize the experimental observations. Both CO and HCOOH formation pathways involve negatively charged intermediates, *i.e.* negatively charged adsorbed CO_2 and adsorbed hydride, resp., whose formation is favored by the interaction with cations. The generation of hydrides is favored by a low metal work function (that correlates with an appropriate position of the metal *d*-band). The cation can further downshift the metal work function by inducing increased surface electronic density and thus promoting hydrides or sustaining the formation of hydrides at high *H coverage. Consequently, CO_2 reduction to formic acid takes place at mild applied potential. Instead, high CO coverages prevent the formation of hydrides both in presence and absence of cations, causing the quick decrease of formic acid selectivity at high applied potential. As a final remark, since cation effects on CO_2RR to HCOOH depend on both the cation accumulation at the surface (well described by cation acidity) and the induced electronic density at the surface, further studies to optimize electrolytes towards formic acid selectivity should target cations (or mixtures) with high induced electric field (*i.e.* $*H^{\delta-}$ favorable formation) and a relatively low acidity, beyond the current employed standard cations (Figure B.12, Table B.3).

Our study reveals once more that the search for optimized systems for CO_2R should carefully tailor the design of both sides of the electrolyte/electrode interface, especially for $HCOOH/HCOO^-$ formation.

References

1. Kuhl, K. P.; Cave, E. R.; Abram, D. N.; Jaramillo, T. F., New insights into the electrochemical reduction of carbon dioxide on metallic copper surfaces. *Energy Environ. Sci.* **2012,** *5* (5), 7050-7059.
2. Hatsukade, T.; Kuhl, K. P.; Cave, E. R.; Abram, D. N.; Jaramillo, T. F., Insights into the electrocatalytic reduction of CO_2 on metallic silver surfaces. *Phys. Chem. Chem. Phys.* **2014,** *16* (27), 13814-9.
3. Min, X.; Kanan, M. W., Pd-catalyzed electrohydrogenation of carbon dioxide to formate: high mass activity at low overpotential and identification of the deactivation pathway. *J. Am. Chem. Soc.* **2015,** *137* (14), 4701-8.
4. Cave, E. R.; Montoya, J. H.; Kuhl, K. P.; Abram, D. N.; Hatsukade, T.; Shi, C.; Hahn, C.; Norskov, J. K.; Jaramillo, T. F., Electrochemical CO_2 reduction on Au surfaces: mechanistic aspects regarding the formation of major and minor products. *Phys. Chem. Chem. Phys.* **2017,** *19* (24), 15856-15863.
5. Cao, Z.; Kim, D.; Hong, D.; Yu, Y.; Xu, J.; Lin, S.; Wen, X.; Nichols, E. M.; Jeong, K.; Reimer, J. A.; Yang, P.; Chang, C. J., A Molecular Surface Functionalization Approach to Tuning Nanoparticle Electrocatalysts for Carbon Dioxide Reduction. *J. Am. Chem. Soc.* **2016,** *138* (26), 8120-5.
6. Zhang, X.; Li, J.; Li, Y. Y.; Jung, Y.; Kuang, Y.; Zhu, G.; Liang, Y.; Dai, H., Selective and High Current CO_2 Electro-Reduction to Multicarbon Products in Near-Neutral KCl Electrolytes. *J. Am. Chem. Soc.* **2021,** *143* (8), 3245-3255.
7. Yuan, X.; Chen, S.; Cheng, D.; Li, L.; Zhu, W.; Zhong, D.; Zhao, Z. J.; Li, J.; Wang, T.; Gong, J., Controllable Cu(0) -Cu(+) Sites for Electrocatalytic Reduction of Carbon Dioxide. *Angew. Chem. Int. Ed. Engl.* **2021,** *60* (28), 15344-15347.
8. Wang, X.; Klingan, K.; Klingenhof, M.; Moller, T.; Ferreira de Araujo, J.; Martens, I.; Bagger, A.; Jiang, S.; Rossmeisl, J.; Dau, H.; Strasser, P., Morphology and mechanism of highly selective Cu(II) oxide nanosheet catalysts for carbon dioxide electroreduction. *Nat. Commun.* **2021,** *12* (1), 1-12.
9. Wuttig, A.; Yaguchi, M.; Motobayashi, K.; Osawa, M.; Surendranath, Y., Inhibited proton transfer enhances Au-catalyzed CO_2-to-fuels selectivity. *Proc. Natl. Acad. Sci. U.S.A.* **2016,** *113* (32), E4585-93.
10. Gao, D.; Zhou, H.; Wang, J.; Miao, S.; Yang, F.; Wang, G.; Wang, J.; Bao, X., Size-dependent electrocatalytic reduction of CO_2 over Pd nanoparticles. *J. Am. Chem. Soc.* **2015,** *137* (13), 4288-91.
11. Guo, R.-H.; Liu, C.-F.; Wei, T.-C.; Hu, C.-C., Electrochemical behavior of CO_2 reduction on palladium nanoparticles: Dependence of adsorbed CO on electrode potential. *Electrochem. Commun.* **2017,** *80*, 24-28.
12. Darby, M. T.; Sykes, E. C. H.; Michaelides, A.; Stamatakis, M., Carbon Monoxide Poisoning Resistance and Structural Stability of Single Atom Alloys. *Top. Catal.* **2018,** *61* (5), 428-438.
13. Arenz, M.; Stamenkovic, V.; Ross, P. N.; Markovic, N. M., Surface (electro-)chemistry on Pt(111) modified by a Pseudomorphic Pd monolayer. *Surf. Sci.* **2004,** *573* (1), 57-66.
14. Baldauf, M.; Kolb, D. M., Formic Acid Oxidation on Ultrathin Pd Films on Au(hkl) and Pt(hkl) Electrodes. *J. Phys. Chem.* **1996,** *100* (27), 11375-11381.
15. Chen, X.; Koper, M. T. M., Mass-transport-limited oxidation of formic acid on a Pd ML Pt(100) electrode in perchloric acid. *Electrochem. Commun.* **2017,** *82*, 155-158.
16. Chen, X.; Granda-Marulanda, L. P.; McCrum, I. T.; Koper, M. T. M., How palladium inhibits

CO poisoning during electrocatalytic formic acid oxidation and carbon dioxide reduction. *Nat. Commun.* **2022,** *13* (1), 38.

17. Wang, H.-X.; Toh, W. L.; Tang, B. Y.; Surendranath, Y., Metal surfaces catalyse polarization-dependent hydride transfer from H_2. *Nat. Catal.* **2023,** *6* (4), 351-362.

18. Huang, B.; Rao, R. R.; You, S.; Hpone Myint, K.; Song, Y.; Wang, Y.; Ding, W.; Giordano, L.; Zhang, Y.; Wang, T.; Muy, S.; Katayama, Y.; Grossman, J. C.; Willard, A. P.; Xu, K.; Jiang, Y.; Shao-Horn, Y., Cation- and pH-Dependent Hydrogen Evolution and Oxidation Reaction Kinetics. *JACS Au* **2021,** *1* (10), 1674-1687.

19. Waegele, M. M.; Gunathunge, C. M.; Li, J.; Li, X., How cations affect the electric double layer and the rates and selectivity of electrocatalytic processes. *J. Chem. Phys.* **2019,** *151* (16), 160902.

20. Ayemoba, O.; Cuesta, A., Spectroscopic Evidence of Size-Dependent Buffering of Interfacial pH by Cation Hydrolysis during CO_2 Electroreduction. *ACS Appl. Mater. Interfaces* **2017,** *9* (33), 27377-27382.

21. Singh, M. R.; Kwon, Y.; Lum, Y.; Ager, J. W., 3rd; Bell, A. T., Hydrolysis of Electrolyte Cations Enhances the Electrochemical Reduction of CO_2 over Ag and Cu. *J. Am. Chem. Soc.* **2016,** *138* (39), 13006-13012.

22. Monteiro, M. C.; Dattila, F.; Hagedoorn, B.; García-Muelas, R.; López, N.; Koper, M., Absence of CO_2 electroreduction on copper, gold and silver electrodes without metal cations in solution. *Nat. Catal.* **2021,** *4* (8), 654-662.

23. Sinha, V.; Khramenkova, E.; Pidko, E. A., Solvent-mediated outer-sphere CO_2 electro-reduction mechanism over the Ag111 surface. *Chem. Sci.* **2022**.

24. Clavilier, J.; Armand, D.; Sun, S. G.; Petit, M., Electrochemical adsorption behaviour of platinum stepped surfaces in sulphuric acid solutions. *J. Electroanal. Chem. Interfacial Electrochem.* **1986,** *205* (1-2), 267-277.

25. Chen, X.; Granda-Marulanda, L. P.; McCrum, I. T.; Koper, M. T. M., Adsorption processes on a Pd monolayer-modified Pt(111) electrode. *Chem Sci* **2020,** *11* (6), 1703-1713.

26. López-Cudero, A.; Cuesta, A.; Gutiérrez, C., Potential dependence of the saturation CO coverage of Pt electrodes: The origin of the pre-peak in CO-stripping voltammograms. Part 1: Pt(111). *J. Electroanal. Chem.* **2005,** *579* (1), 1-12.

27. Kortlever, R.; Peters, I.; Koper, S.; Koper, M. T. M., Electrochemical CO_2 Reduction to Formic Acid at Low Overpotential and with High Faradaic Efficiency on Carbon-Supported Bimetallic Pd–Pt Nanoparticles. *ACS Catal.* **2015,** *5* (7), 3916-3923.

28. Kresse, G.; Furthmuller, J., Efficient iterative schemes for ab initio total-energy calculations using a plane-wave basis set. *Phys. Rev. B: Condens. Matter* **1996,** *54* (16), 11169-11186.

29. Kresse, G.; Furthmüller, J., Efficiency of ab-initio total energy calculations for metals and semiconductors using a plane-wave basis set. *Comput. Mater. Sci.* **1996,** *6* (1), 15-50.

30. Perdew, J. P.; Burke, K.; Ernzerhof, M., Generalized Gradient Approximation Made Simple. *Phys. Rev. Lett.* **1996,** *77* (18), 3865-3868.

31. Grimme, S., Semiempirical GGA-type density functional constructed with a long-range dispersion correction. *J. Comput. Chem.* **2006,** *27* (15), 1787-99.

32. Bucko, T.; Hafner, J.; Lebegue, S.; Angyan, J. G., Improved description of the structure of molecular and layered crystals: ab initio DFT calculations with van der Waals corrections. *J. Phys. Chem. A* **2010,** *114* (43), 11814-24.

33. Almora-Barrios, N.; Carchini, G.; Blonski, P.; Lopez, N., Costless Derivation of Dispersion

Coefficients for Metal Surfaces. *J. Chem. Theory Comput.* **2014,** *10* (11), 5002-9.

34. Kresse, G.; Joubert, D., From ultrasoft pseudopotentials to the projector augmented-wave method. *Phys. Rev. B* **1999,** *59* (3), 1758-1775.

35. Blochl, P. E., Projector augmented-wave method. *Phys. Rev. B: Condens. Matter* **1994,** *50* (24), 17953-17979.

36. Monteiro, M. C. O.; Dattila, F.; Lopez, N.; Koper, M. T. M., The Role of Cation Acidity on the Competition between Hydrogen Evolution and CO_2 Reduction on Gold Electrodes. *J. Am. Chem. Soc.* **2022,** *144* (4), 1589-1602.

37. Dattila, F.; Monteiro, M. C. O.; Koper, M. T. M.; López, N., Reply to: On the role of metal cations in CO_2 electrocatalytic reduction. *Nat. Catal.* **2022,** *5* (11), 979-981.

38. Makov, G.; Payne, M. C., Periodic boundary conditions in ab initio calculations. *Phys. Rev. B: Condens. Matter* **1995,** *51* (7), 4014-4022.

39. Marcus, Y., Ionic radii in aqueous solutions. *Chem. Rev.* **1988,** *88* (8), 1475-1498.

40. Chan, K.; Nørskov, J. K., Electrochemical Barriers Made Simple. *J. Phys. Chem. Lett.* **2015,** *6* (14), 2663-2668.

41. Chan, K.; Nørskov, J. K., Potential Dependence of Electrochemical Barriers from ab Initio Calculations. *J. Phys. Chem. Lett.* **2016,** *7* (9), 1686-1690.

42. Daniele, S.; Baldo, M. A.; Corbetta, M.; Mazzocchin, G. A., Linear sweep and cyclic voltammetry for metal deposition at solid and mercury microelectrodes from solutions with and without supporting electrolyte. *J. Electroanal. Chem.* **1994,** *379* (1-2), 261-270.

43. Bard, A. J.; Faulkner, L. R.; White, H. S., *Electrochemical Methods: Fundamentals and Applications*. Wiley: 2022.

44. Goyal, A.; Koper, M. T. M., The Interrelated Effect of Cations and Electrolyte pH on the Hydrogen Evolution Reaction on Gold Electrodes in Alkaline Media. *Angew. Chem. Int. Ed. Engl.* **2021,** *60* (24), 13452-13462.

45. Bellarosa, L.; Garcia-Muelas, R.; Revilla-Lopez, G.; Lopez, N., Diversity at the Water-Metal Interface: Metal, Water Thickness, and Confinement Effects. *ACS Cent. Sci.* **2016,** *2* (2), 109-116.

46. Diercks, J. S.; Georgi, M.; Herranz, J.; Diklić, N.; Chauhan, P.; Clark, A. H.; Hübner, R.; Faisnel, A.; Chen, Q.; Nachtegaal, M.; Eychmüller, A.; Schmidt, T. J., CO_2 Electroreduction on Unsupported PdPt Aerogels: Effects of Alloying and Surface Composition on Product Selectivity. *ACS Appl. Energy Mater.* **2022,** *5* (7), 8460-8471.

47. Sumaria, V.; Nguyen, L.; Tao, F. F.; Sautet, P., Optimal Packing of CO at a High Coverage on Pt(100) and Pt(111) Surfaces. *ACS Catal.* **2020,** *10* (16), 9533-9544.

48. Liu, X.; Monteiro, M. C. O.; Koper, M. T. M., Interfacial pH measurements during CO_2 reduction on gold using a rotating ring-disk electrode. *Phys. Chem. Chem. Phys.* **2023,** *25* (4), 2897-2906.